DOI: 10.13009/EUCASS2023-262
Aerospace Europe Conference 2023 – 10TH EUCASS – 9TH CEAS

Characterisation of thermal management system specific heat rejection for electric propulsion architectures

Antje Link⋆†, *Martin Staggat*⋆ *and Stefanie de Graaf*⋆
⋆ *DLR Institute of Electrified Aero Engines*
Lieberoser Straße 13A, 03046 Cottbus, Germany
antje.link@dlr.de
†Corresponding author

Abstract

A thermal management system (TMS) is required to manage the heat loads of aircraft electric powertrain components. The specific heat rejection is used to describe the mass penalty of the TMS. A liquid cooled generic TMS architecture is defined with its components either modelled analytically or based on empirical scaling expressions. The TMS specific heat rejection is evaluated across various input parameters such as the heat flow, the fluid temperatures and the pipe dimensions. As a result trade-off options can be identified to reduced the overall system mass and are used to define design recommendations for TMSs to increase the specific heat rejection.

1. Introduction

To limit the climate impact of aviation, electrified aircraft propulsion concepts are identified as one possible pathway as illustrated by Waypoint 2050 [1]. Such electrified propulsion architectures introduce electric components to the propulsion system which reject heat at low temperature levels. In the absence of conventional heat sinks such as kerosene and the engine bypass flow, the introduction of an actively managed Thermal Management System (TMS) imposes further challenges as the TMS leads to additional mass, power and drag penalties within the overall aircraft design process [2].

To capture the TMS mass penalty within the design process, the TMS mass is either derived by explicit modelling of the TMS and its components in detail or by using a scaling factor correlating the heat managed by the TMS to its total mass. If provided explicitly within literature, the relationship between heat managed by the TMS and its associated mass has a variety of designations. Its names range from power or heat density [3], combined specific cooling (CSC) [4], to specific heat rejection [5, 6].

At aircraft preliminary design level TMS effects are being considered by using fixed specific heat rejection values to account for the TMS mass penalty [7, 8]. In more recent studies more detailed TMS modelling approaches capture components individually to consider the parasitic TMS effects more accurately [9–11]. In-depth investigations of the TMS architectures and their sensitivities have been carried out to understand the system behaviour and the characteristics of parasitic effects in more detail [4–6, 12, 13]. While designing the TMS requires an understanding of both, the propulsion system architecture as well as aircraft integration, correlations to include the effects of TMS with reasonable accuracy but without the need for a detailed TMS modelling would improve the accuracy during the preliminary design process.

Lents [3] summarises the TMS mass penalty of previous works [9, 10] and derives their associated specific heat rejection. The evaluated investigations cover hybrid-electric powertrains for single aisle aircraft applications and achieve a specific heat rejection of $1\,\mathrm{kW\,kg^{-1}}$ to $2\,\mathrm{kW\,kg^{-1}}$ for state of the art TMS. While a specific heat rejection of $2\,\mathrm{kW\,kg^{-1}}$ is assumed appropriate for electric powertrain components, low temperature battery heat results in a lower specific heat rejection of $1\,\mathrm{kW\,kg^{-1}}$. The considered components include the Heat Exchanger (HEX), fans and motors to drive the fans but does not consider plumbing and pumps for which an additional penalty of 20 % is being recommended by Lents [3]. This effectively yields reduced specific heat rejection values of $0.83\,\mathrm{kW\,kg^{-1}}$ to $1.67\,\mathrm{kW\,kg^{-1}}$.

Chapman *et al.* [12] describe a detailed TMS design used for a VTOL tiltwing application. The investigation provides a modelling framework for a liquid-cooled TMS and addresses the combined optimisation of weight, power utilisation and drag penalties associated to the TMS. The TMS considers components such as the HEX, the pipes as well as the coolant pump and the puller fan mass. Of specific interest are the presented studies for heat exchanger

DOI: 10.13009/EUCASS2023-262

optimisation which illustrate the trade-off between mass and power required for varied heat flow rejection or air temperature values. Chapman *et al.* [13] continue their investigation [12] for different TMS sizes. Initially, the TMS design sensitivities with respect to the rejected power and temperature limits are explored. TMSs for three different aircraft concepts spanning urban air mobility, regional and narrowbody aircraft sizes are investigated considering both current state of the art as well as future technology based TMS concepts. Scaling expressions for each of the different applications and TMS concepts are derived correlating the rejected heat load to mass, parasitic power and drag of the TMS. While the TMS of individual electric components manage head loads of less than 200 kW, their corresponding specific heat rejection values can be post-processed from the results provided and range from 1.25 $\mathrm{kW\,kg^{-1}}$ to 5 $\mathrm{kW\,kg^{-1}}$.

Gkoutzamanis *et al.* [4] investigate the TMS for a hybrid-electric commuter aircraft application. The designed TMS considers the heat exchanger, pipes, coolant and tank, pump and associated cold plates. The HEX is modelled based on porosity assumptions with the available heat transfer area and associated heat transfer coefficient treated as an input parameter. Sensitivity studies addressing the impact of system characteristics, such as pipe diameters and heat loads on the TMS mass, are carried out while also addressing redundancy and uncertainty calculations. The designed system achieves a specific heat rejection of 0.79 $\mathrm{kW\,kg^{-1}}$.

Link *et al.* [5] describe a combined fuel cell and TMS optimisation. The implemented simplified TMS layout considers key components such as coolant, heat exchanger and a compressor using a simple modelling approach. A reserve factor of 20 % is used to account for not modelled but required system components. For the design point at static maximum-take off condition a trade-off study has been carried out linking the TMS and fuel cell sizing processes to mass and power demand for a dedicated serial cooling concept. The derived specific heat rejection values range from 1.64 $\mathrm{kW\,kg^{-1}}$ to 2.93 $\mathrm{kW\,kg^{-1}}$ for a fuel cell TMS.

Webber *et al.* [6] provide a roadmap for fuel cell related heat exchanger technology development. A projection for the TMS specific heat rejection covering the years 2026, 2035 and 2050 is provided with ranges from 5 $\mathrm{kW\,kg^{-1}}$ to 20 $\mathrm{kW\,kg^{-1}}$ at system level considering both fuel cell type and TMS architecture developments.

As a consequence of this review, the TMS designs and thus their associated specific heat rejections are not necessarily transferable between different propulsion architectures as different electrical components require different TMS strategies due to their individual operating conditions such as heat flows and temperatures. Additionally, within the presented assessments there remain deviations in both, the modelling assumptions of TMS components as well as the selection of considered TMS components. This complicates the direct comparability of the available TMS specific heat rejection values across different propulsion architectures and sizes.

In this paper, a generic TMS architecture and its constituting components are defined in section 2. Either analytical or empirical scaling expressions are being used for each of the components. In addition, both the input parameter variation as well as the output metrics are defined. Within section 3, the results of the sensitivity study are presented across a range of input parameter variations reflecting electric propulsion applications for aviation. This also includes a discussion on trade-off characteristics and TMS design recommendations. Subsequently in section 4, the results are compared to available studies within literature. The paper concludes in section 5 with a summary and recommendations for further work.

2. Methods

2.1 Thermal Management System Architecture

To evaluate the TMS independently from the detailed electric powertrain design, a generic TMS architecture for a liquid based system is defined and shown in Figure 1. The required components are derived based on the key functions of the Thermal Management System – namely: the heat pick-up at the source of the heat generation as well as heat transport and subsequent heat rejection to ambient air. This generic layout of the TMS allows a design space exploration of the TMS across a range of different operating conditions to identify key drivers and behaviours of the TMS sizing. This enables initial estimates for the TMS size with limited detailed design knowledge of the aircraft and propulsion system.

With regard to the mass of the TMS, this leads to the following key TMS components: coolant, heat exchanger, coolant pump, pipes and puller fan for air supply if required by the operating condition. The mass of those contributors are either taken from literature or derived analytically and are described in more detail in the next section. Any additional elements required for heat pick-up within the heat source are associated to the heat source – such as the cold plate of power electronics or cooling channels within a fuel cell – and are not considered part of the TMS from a mass breakdown perspective.

From a performance perspective of the TMS, the pressure losses within both the liquid as well as the air system need to be described. In addition to the heat exchanger and pipes, this may include the pressure drop of the fluid at the heat source, as well as additional information on the air pressures within the ram air channel.

DOI: 10.13009/EUCASS2023-262

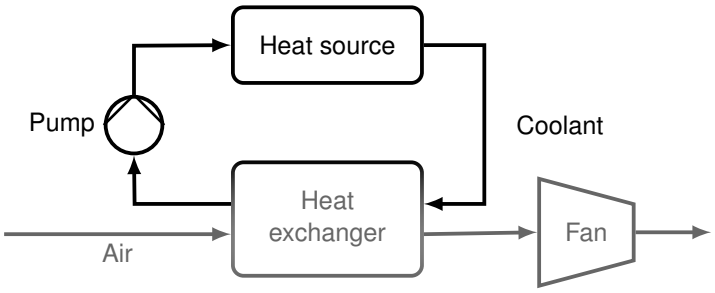

Figure 1: Generic TMS architecture

While the identified components of the TMS are each modelled individually, both pump and fan calculation are linked to the pipe and heat exchanger calculations as key drivers for the associated pressure drops within the fluids. Similarly, the coolant circulation time within heat exchanger and pipe influences the coolant mass.

2.2 Component Modelling

For each of the identified TMS components, a sizing calculation is carried out to derive the mass of the individual component. In addition, the component specific pressure losses are calculated to enable the calculation of the required power penalty for the TMS.

Coolant

Based on the heat flow rate $\dot{Q}$ defined by

$$\dot{Q} = \dot{m} c_p \Delta T \ , \tag{1}$$

the coolant mass flow $\dot{m}$ is calculated assuming a given fluid type and thus specific heat capacity c_p as well as a given temperature difference ΔT based on the operating temperatures of the heat source. For the selected fluid, all required fluid material properties were extracted from the *CoolProp* library [14].

The coolant mass m_{HF} is derived from the required coolant mass flow rate $\dot{m}_{HF}$ and its total circulation time Δt_{circ} within all system components as

$$m_{HF} = \dot{m}_{HF} \sum \Delta t_{circ} \ , \tag{2}$$

where the coolant is referred to as Hot Fluid (HF) while the air will be referred to as Cold Fluid (CF). Hereby, the circulation time t_{circ} depends on the geometric length of the piping and HEX and the assumed velocity of the fluid.

Pipe

Based on the coolant mass flow rate $\dot{m}_{HF}$, the pipe mass m_{pipe}, the fluid velocity within the pipe v_{HF} as well as the pipe pressure drop Δp are calculated. The pipe mass m_{pipe} is hereby described by

$$m_{pipe} = \frac{\pi}{4} \left(d_a^2 - d_i^2 \right) l \rho_{pipe} \ , \tag{3}$$

using its geometric dimensions, i.e. its outer and inner diameters d_a and d_i as well as its length l and its material density ρ_{pipe}. The fluid velocity within the pipe v_{HF} and the system in general given by

$$v_{HF} = \frac{\dot{m}_{HF}}{\frac{\pi}{4} d_i^2 \rho_{HF}} \ , \tag{4}$$

is calculated based on the coolant mass flow rate $\dot{m}_{HF}$, the fluid density ρ_{HF} and the inner cross sectional area of the pipe which is calculated based on the pipe inner diameter d_i.

Based on friction factor correlation data, the pressure drop for a smooth pipe is derived by

$$\Delta p = 2 f \rho v_{HF}^2 \frac{l}{d_i} \ , \tag{5}$$

with its geometric parameters l and d_i and the known fluid velocity v_{HF}. Morrison [15] derived a correlation for the Fanning friction factor

$$f = \left(\frac{0.0076 \left(\frac{3170}{Re} \right)^{0.165}}{1 + \left(\frac{3170}{Re} \right)^{7.0}} \right) + \frac{16}{Re} \ , \tag{6}$$

DOI: 10.13009/EUCASS2023-262

which correlates the friction factor f to the pipe Reynolds number Re which approximates both laminar and transient regimes.

Heat exchanger

The Heat Exchanger (HEX) layout consists of an offset strip finned air side as well as a liquid side with rectangular tubes as illustrated in Figure 2a. This HEX design is selected to increase compactness for the air side while maintaining simplicity for the liquid side.

The thermal performance calculations of a heat exchanger is typically based on the ε-NTU method described by Kays and London. This method characterises the heat exchanger based on an effectiveness ε and the number of transfer units NTU and allows to determine the product of the total heat transfer coefficient U and the heat transfer area A as a characteristic HEX parameter UA. To calculate the HEX mass, the parameter UA needs to be transferred into actual HEX dimensions.

The HEX sizing calculation follows a cell scaling approach for preliminary HEX design calculations proposed by Bachmann *et al.* [17]. The cell scaling approach defines the smallest cell of a HEX as one finned air passage and its liquid passage beneath. The cell dimension parameter nomenclature follows the definitions by Shah and Sekulic [18] and is illustrated in Figure 2b. The model implemented for this study deviates from Bachmann *et al.* [17] primarily in two aspects: 1) a simplification of the geometry of the liquid side channel to a rectangular channel and 2) in the determination of the air side pressure loss solely based on the through flow length.

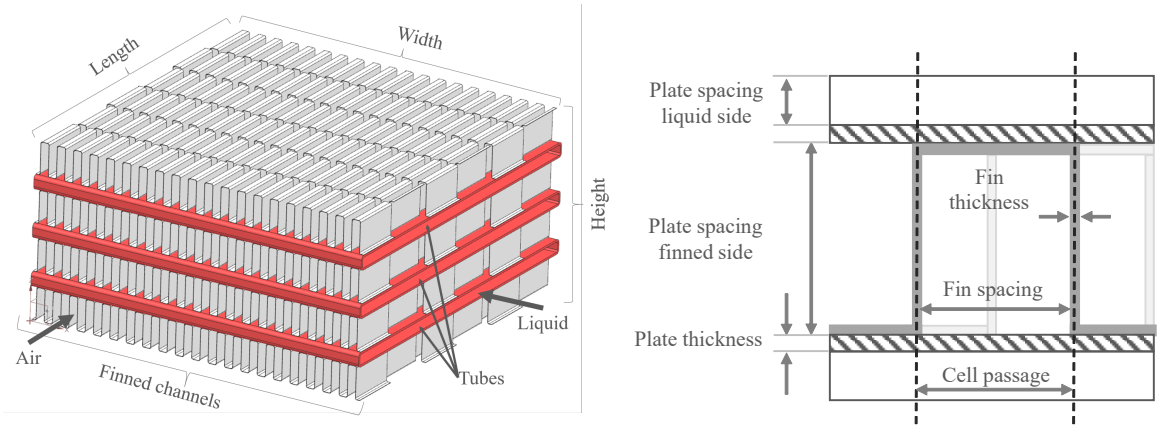

(a) Offset-Strip Fin HEX architecture

(b) HEX cell nomenclature

Figure 2: Heat exchanger architecture and nomenclature

The HEX cell scaling approach is split into three main steps that are also illustrated in Figure 3:

1. Thermal performance calculation according to the ε-NTU method introduced by Kays and London [16] to calculate UA_{req} required for a dedicated heat load and temperature inputs.

2. Characterisation of a single heat exchanger cell, and calculation of the heat transfer coefficient within a cell to determine UA_{cell} at cell level.

3. Scaling cell results to the total heat exchanger requirements and determine heat exchanger dimensions, mass, volume as well as pressure losses.

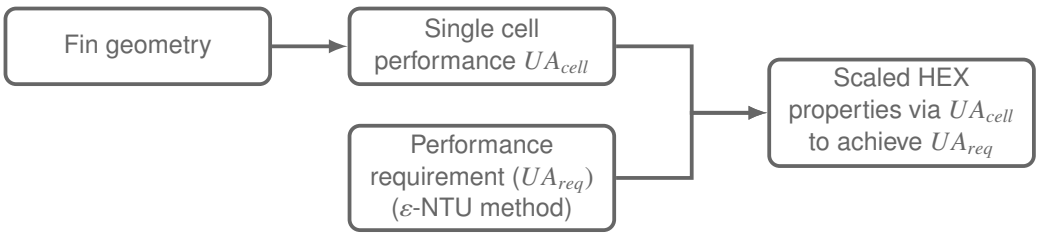

Figure 3: HEX sizing calculation

DOI: 10.13009/EUCASS2023-262

Based on the geometric definitions of the single HEX cell as given in Figure 2b, its mass is derived by

$$m_{cell} = \rho_{mat} \left((s + b_1)\, \delta L_f + 2\,(s + \delta)\, \delta_W \left(L_f + b_2 \right) \right) , \tag{7}$$

using its geometric parameters – namely: L_f as HEX air side length corresponding to the overall HEX length, the plate spacing of the finned side b_1 and the plate spacing of the liquid side b_2, the fin spacing s, the fin thickness and δ and plate thickness δ_W, as well as the HEX material density ρ_{mat}.

Subsequently, the single cell mass is scaled through

$$m_{HEX} = m_{cell} \frac{UA_{req}}{UA_{cell}} , \tag{8}$$

via the relationship of UA_{req} from the thermal performance requirement to the UA_{cell} achieved within the cell.

The pressure drop for each of the fluids is approximated similarly to the pipe pressure drops presented in Equation 5 while properly accounting for the fluid densities and velocities as well as passage lengths and hydraulic diameters. Any entry and exit effects of the flows to the heat exchanger are neglected. For the Colburn and Fanning friction factors of the offset strip fin air passages, correlations derived by Manglik and Bergles [19] were used.

Pump

To ensure circulation of the coolant, a pump is needed to overcome the pressure drop within the coolant system. The parasitic power required to operate the pump P_{pump} is calculated with the coolant volume flow $\dot{V}_{HF}$, the pump efficiency η_{pump} and the total pressure drop Δp_{total} across all system components through

$$P_{pump} = \frac{\dot{V}_{HF} \sum \Delta p_{total}}{\eta_{pump}} , \tag{9}$$

where η_{pump} is the efficiency of the pump. Manufacturers' data for engine oil [20] and fuel pumps [21] has been used to derive the following correlation between volume flow rate and pump mass:

$$m_{pump} = 3294.1 \dot{V}_{HF} + 3.0944 . \tag{10}$$

The curve fit of this correlation is illustrated in Figure 4a. Compared to the correlation provided by Chapman *et al.* [12], which has been used in other studies [4] as well, this yields a significant reduction in pump weight for large volume flows. However, both Chapman *et al.* [12] as well as Gkoutzamanis *et al.* [4] only use this correlation for comparably low fluid volume flows. Applying it to higher volume flow rates might simply exceed the intended application range of the correlation.

While the data used to derive the correlation represents aviation specific pump applications, there is still an uncertainty whether the data is appropriate for electrically driven coolant pumps. Data from automotive coolant pumps [22] is only available for comparably small coolant flow rates but still highlights the potential for even lower component mass.

Puller Fan

From a performance perspective, the electric power for compression P_{fan} is described by

$$P_{fan} = \frac{1}{\eta_{el}} \dot{m}_{CF} c_p \Delta T , \tag{11}$$

linking the mass flow $\dot{m}_{CF}$, the specific heat capacity c_p, the isentropic temperature difference ΔT due to the compression as well as an electric efficiency η_{el} to translate the mechanical power required for compression to the power requirement for an electric motor which drives the fan. The isentropic state of change is further described by

$$\Delta T = \frac{1}{\eta_{is}} T_{fan_{in}} \left(\Pi^{\frac{\kappa-1}{\kappa}} - 1 \right) , \tag{12}$$

using a constant isentropic efficiency η_{is} and isentropic exponent κ, an inlet air temperature $T_{fan_{in}}$ and a fan pressure ratio Π. Herein, the fan pressure ratio compensates all system pressure losses related to the air path, such as inlet and exit losses as well as the pressure loss within the heat exchanger.

In literature, fan mass correlations employ either a scaling by the fan mass flow [12] or by the required power for compression [11]. Data sources range from manufacturers' data sheets as used by Chapman *et al.* [12] to compressor

DOI: 10.13009/EUCASS2023-262

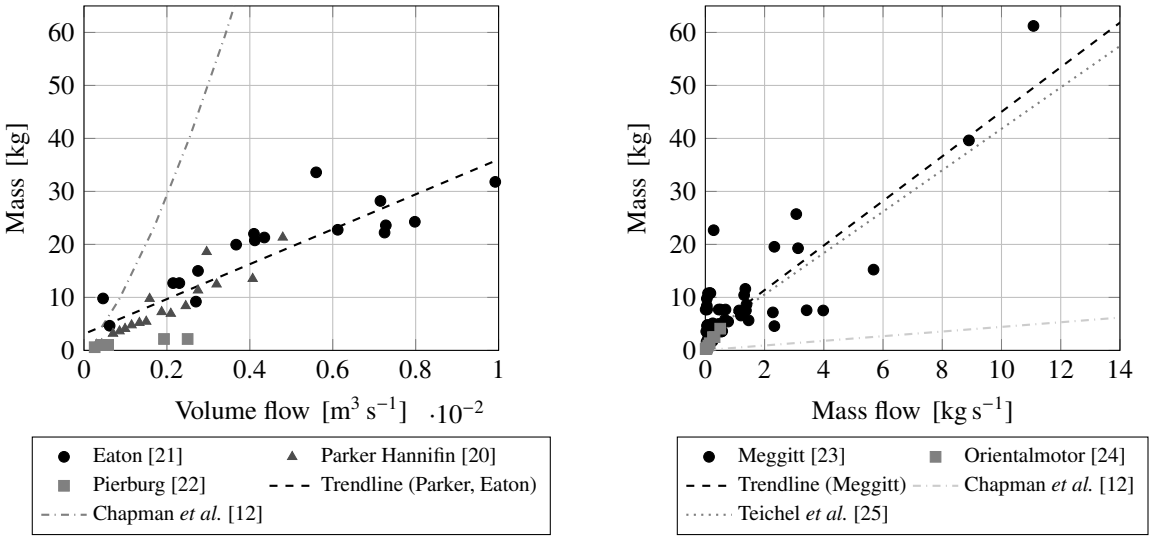

(a) Pump data and correlations

(b) Fan data and correlations

Figure 4: Empirical correlations of pump and fan mass to respective flow rates

design mass predictions as used by Palladino *et al.* [11]. Both manufacturer data for aerospace fans [23] as well as electric fans [24] (MRS and MU series), to data calculated by Teichel *et al.* [25] are plotted in Figure 4b.

Based on the Meggitts' manufacturer data sheets Meggitt Defense Systems, the following correlation between air mass flow and fan mass has been derived:

$$m_{fan} = 4.2054\dot{m}_{CF} + 2.9707\ . \tag{13}$$

The results obtained are similar to those of Teichel *et al.* [25] while a significant deviation to the scaling expression derived by Chapman *et al.* [12] was observed. While this expression is derived based on mass flow rates of up to $11\,\mathrm{kg\,s^{-1}}$, most of the data is limited to $5\,\mathrm{kg\,s^{-1}}$. Any extrapolation results exceeding mass flows of $11\,\mathrm{kg\,s^{-1}}$ need to be treated with according caution.

As the investigation currently focuses on calculations at sea level, the mass flow rate has been selected as an appropriate scaling factor. Alternative scaling factors, such as the power for compression or the volume flow rate, could also be used depending on the sizing point within the mission.

2.3 Variation Parameters and Post-Processing Metrics

The heat source and its associated operating condition are key drivers for sizing the coolant fluid, heat exchanger and puller fan. Integration and propulsion system architecture design, i.e. the location of components to one another, influences both the pipes as well as the coolant fluid.

The variation parameters include the rejected heat flow, the coolant fluid type and its associated specific heat capacity, the coolant temperature difference for heat pickup and the air temperature difference within the heat exchanger which is described by the temperature effectiveness as well as pipe diameters and lengths. At the same time, no optimisation over the finned geometry within the heat exchanger is carried out. The parameter ranges are provided in Table 1.

Parameter	Symbol	Unit	Min Value	Max Value
Heat flow	$\dot{Q}$	kW	100	1000
Operating temperature coolant	T_{HF}	°C	60	180
Temperature difference coolant	ΔT_{HF}	K	10	50
Temperature effectiveness	ε_T	-	0.3	0.9
Pipe length	l_{pipe}	m	2	20
Pipe diameter	d_{pipe}	m	0.025	0.10

Table 1: Ranges of investigated parameters

DOI: 10.13009/EUCASS2023-262

The air and coolant temperature and their associated temperature differences within the heat exchanger are related as the air temperature cannot exceed the coolant temperature entering the heat exchanger. The relationship between the temperature differences is described by the temperature effectiveness ε_T. In case of air being the fluid with the minimum heat capacity rate $\dot{C}_{min} = \left(\dot{m}c_p\right)_{min}$, the defined temperature effectiveness corresponds to the effectiveness of the heat exchanger as defined by the ε-NTU method. An ambient temperature of 30 °C is assumed which corresponds to an ISA+15K day condition.

Coolant fluids ranging from heat transfer fluids such as DOWTHERM Q and Dynalene HC50 to Water-Ethylene-Glycol mixtures with specific heat capacities ranging from 2200 J kg^{-1} K^{-1} to 3500 J kg^{-1} K^{-1} have been considered based on the *CoolProp* library [14] depending on their operating temperature ranges.

A design space investigation has been carried out covering a broad range of parameter values. Some parameter combinations might yield unrealistic results, such as high coolant flows through pipes with small diameters resulting in high pressure losses or low coolant flows through pipes with large diameters result in flows with very low Reynolds numbers. Those cases have been addressed within an according error handling procedure.

Primary focus of the study is the characterisation of the specific heat rejection provided by

$$SHR = \frac{\dot{Q}}{m}\,, \tag{14}$$

which is calculated at TMS level based on the rejected heat $\dot{Q}$ and the system total mass m.

As a secondary parameter the TMS power ratio η_{TMS} is derived by

$$\eta_{TMS} = \frac{P_{el}}{\dot{Q}}\,, \tag{15}$$

and characterises the relationship between the electric power required P_{el} and the rejected heat $\dot{Q}$.

While a higher specific heat rejection value represents a lower TMS mass for a given heat flow, a lower TMS power ratio indicates a lower level of power required to reject the heat. Both, high specific heat rejection and low TMS power ratio values are therefore considered beneficial to the system design.

3. Results

3.1 Single Parameter Variation

To understand and validate the initial system behaviour, a sensitivity study was carried out varying the identified input parameters individually, while keeping the remaining parameters constant. This study explores the parameter limits provided in Table 1 individually and generally considers the average of the provided minimum and maximum values as baseline input parameters within the assessment. Only the pipe diameter has been treated differently, due to its impact on physical model restraints: its baseline value has been assumed as 0.05 m and its variation explores diameter ranges from 0.05 m to 0.1 m.

The specific heat rejection was calculated for this parameter variation and its deviation to the baseline case is illustrated in Figure 5. As this investigation covers a large range of applicable temperatures which exceed the temperature range of Water-Ethylene-Glycol, a heat transfer fluid such as DOWTHERM Q is considered for the investigations.

Varying only one system parameter, while keeping all others the same, a positive correlation can be observed between the specific heat rejection and the heat flow, the operating temperature of the hot fluid, the temperature difference of the hot fluid across the HEX as well as the temperature effectiveness as illustrated by Figures 5a to 5d. The latter implicitly represents the temperature difference of the cold fluid across the HEX. For increasing pipe diameter or length, the specific heat rejection decreases as shown in Figure 5e and 5f.

By increasing the heat flow the size of components such as the HEX, the fan and the pump increases. While an increase in heat flow directly leads to an increase in fluid mass flow, the increase of the component masses is not directly proportional to it, when using the derived scaling expressions (Equation 10 and 13) and modelling. For example, an increase by a factor of ten in the heat flow and thus the fluid mass flows, leads to a lower increase in fan and pump masses.

An increase in operating temperature T_{HF} leads to a significant size reduction of the fan and the heat exchanger and therefore an increased specific heat rejection.

For lower input parameters values of pipe lengths and diameters, a higher specific heat rejection value is observed which is driven by an increased amount of hot fluid in the system. This highlights the need to integrate the TMS as good as possible to reduce the required piping and hot fluid mass.

DOI: 10.13009/EUCASS2023-262

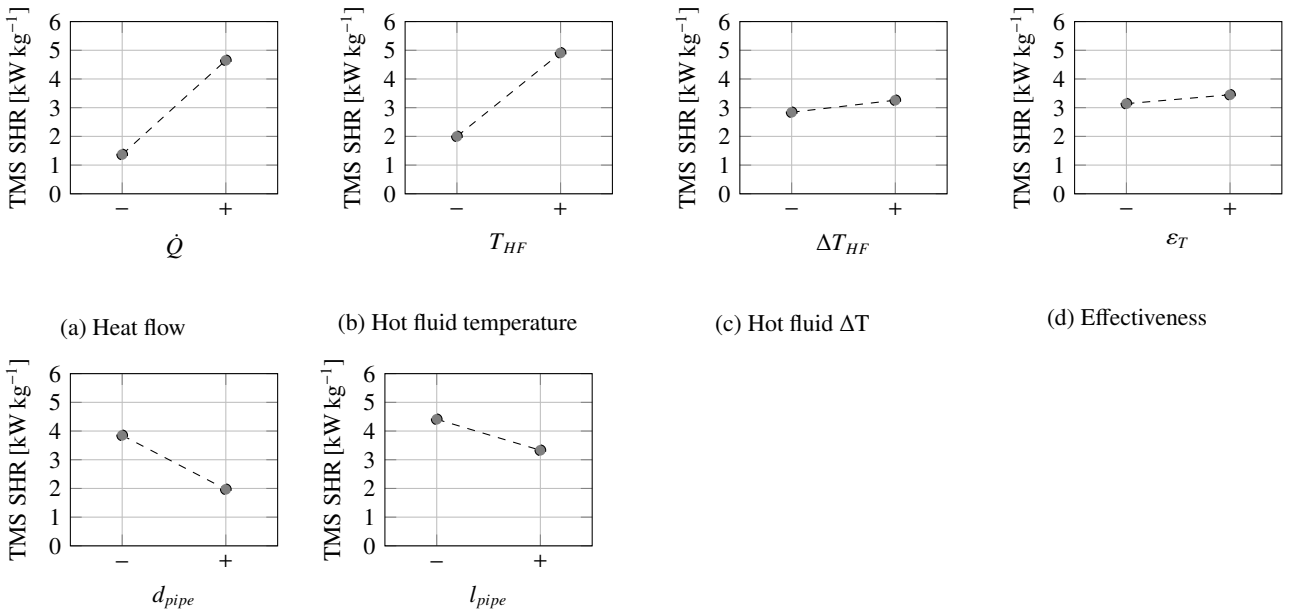

(a) Heat flow (b) Hot fluid temperature (c) Hot fluid ΔT (d) Effectiveness

(e) Pipe diameter (f) Pipe length

Figure 5: Individual parameter effect on specific heat rejection

And detailed study for a heat flow of $\dot{Q}$ =300 kW enables a closer look at the temperature differences of the fluids across the HEX within the system which reveals a trade-off between the system component mass contributions to maximise the specific heat rejection which is illustrated in Figure 6. The temperature differences of both fluids, characterised by either the temperature difference directly or indirectly via the temperature effectiveness, show highest values for the specific heat rejection for intermediate parameter values. This behaviour is driven by the individual mass contributors illustrated in Figure 7.

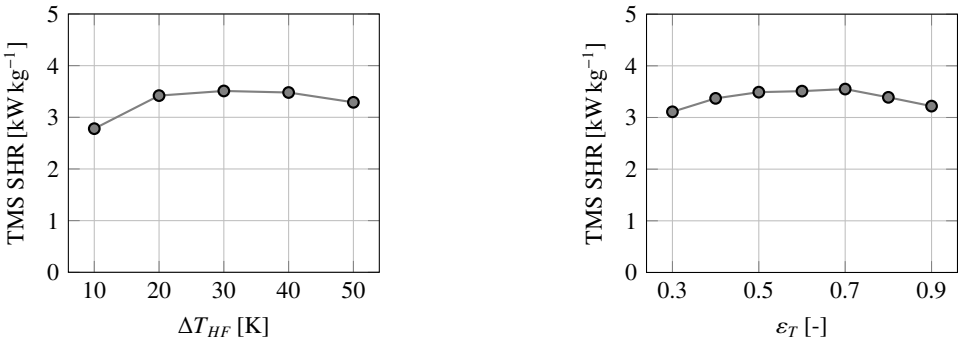

(a) SHR for hot fluid ΔT variation (b) SHR for effectiveness variation

Figure 6: Impact of hot and cold fluid temperature parameterisation on specific heat rejection

For the hot fluid temperature difference across the HEX, this is caused by a trade-off between the hot fluid related components, i.e. the heat exchanger, the pump as well as the hot fluid mass itself which is illustrated in Figure 7a . An increase in temperature difference affects three aspects of the TMS. Firstly, the hot fluid mass flow reduces and thus less volume flow leads to a smaller pump sizing according to Equation 10. Secondly, the heat exchanger mass increases to account for the additional heat transfer area required on the liquid side to meet the required heat flow across the heat exchanger. Lastly, the total fluid mass increases due to the constant pipe dimensions with subsequent impact on the velocity within the system and thus leads to a longer fluid circulation time.

Similarly, for the temperature effectiveness a trade-off between the related components on the air side was observed and is shown in Figure 7b. Here, an increase in assumed temperature effectiveness and thus an increased air temperature difference causes an increase in heat transfer area. While this leads to an increase in heat exchanger mass,

DOI: 10.13009/EUCASS2023-262

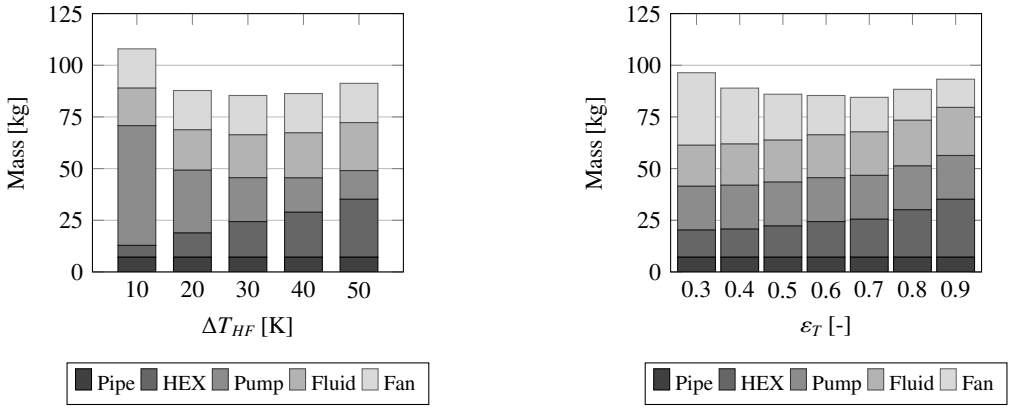

(a) Mass contributors for hot fluid ΔT variation

(b) Mass contributors for effectiveness variation

Figure 7: Impact of hot and cold fluid temperature parameterisation on individual component mass contributors

at the same time less air mass flow is required based on the heat flow equation (Equation 1). Due to the fan mass scaling as per Equation 13, this leads to a reduction in fan mass.

3.2 Multi parameter variation

Figure 8 illustrates the combined parameter variation of the temperature effectiveness at air side and hot fluid temperature difference for the liquid side for a heat flow of $\dot{Q}$ =300 kW. Results are shown for a hot fluid temperature of 120 °C in Figure 8a and 160 °C in Figure 8b.

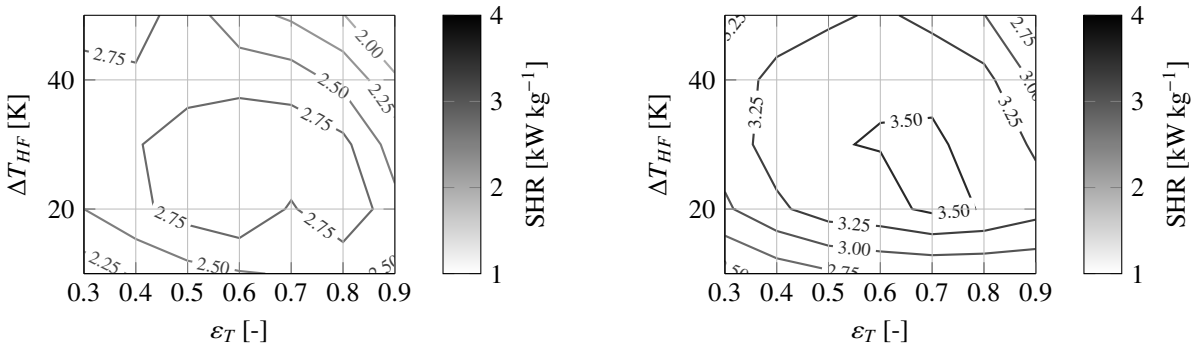

(a) TMS specific heat rejection at T=120 °C

(b) TMS specific heat rejection at T=160 °C

Figure 8: Variation of hot fluid temperature difference and air-side temperature effectiveness for defined hot fluid temperature levels

The results illustrated in Figure 8 illustrate a maximum of the specific heat rejection occurs within a temperature difference of 20 K to 30 K for the hot fluid and a temperature effectiveness of 0.5 to 0.8 for T_{HF} =120 °C and 0.6 to 0.7 for T_{HF} =160 °C respectively.

This is a result of the two previously observed effects in Figure 6 and highlights the need for a holistic TMS assessments including all relevant TMS components to reduce the total system mass and thus maximise the specific heat rejection. Increasing the hot fluid temperature level leads to higher achievable specific heat rejection values. Both operating temperatures show a wide plateau for the specific heat rejection and therefore illustrate the design space for acceptable solutions with limited impact on the specific heat rejection.

Similarly, varying the temperature effectiveness as well as the hot fluid temperature level while keeping the temperature difference ΔT=30 K illustrates the trade-off between both specific heat rejection and system power ratio as shown in Figure 9.

While the specific heat rejection shown in Figure 9a increases with increasing hot fluid temperature, a reduction in TMS power ratio is coupled to both input parameters and is shown in Figure 9b.

DOI: 10.13009/EUCASS2023-262

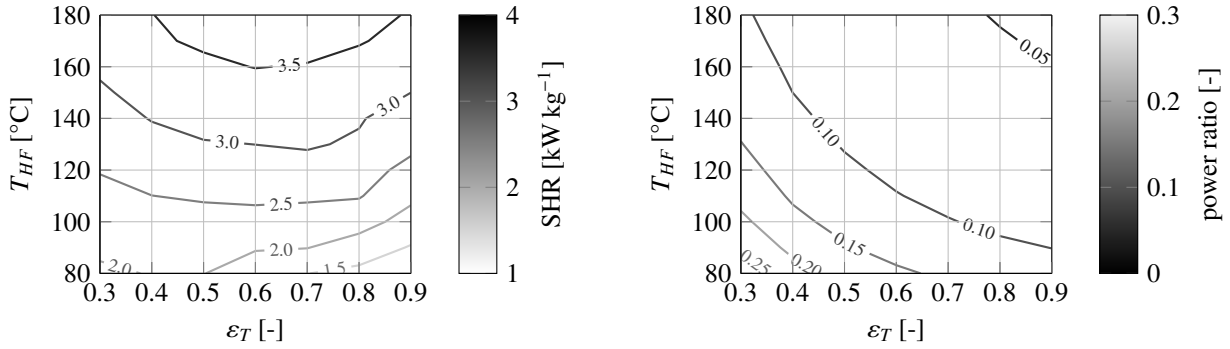

(a) TMS specific heat rejection

(b) TMS power ratio

Figure 9: Variation of hot fluid temperature and temperature effectiveness for ΔT_{HF}=30 K

Especially for low hot fluid temperatures, the highest specific heat rejection is achieved at the expense of a high power demand to enable the TMS operation. At higher operating temperatures, this penalty becomes less relevant and the TMS power ratio values are below 0.1 to 0.15.

3.3 Scaling Approximations

While it is possible to use single parameter scaling expressions for a fixed design as used by Chapman *et al.* [13], it has to be noted that those scaling expressions are specific to the designed TMS application case and cannot be easily transferred to other application cases.

The scatter and sensitivity to results shown in Figure 10 illustrates why approaching the TMS specific heat rejection and thus TMS mass as a single factor based scaling expressions is not applicable from a generic TMS architecture point of view. For all variation parameters, the specific heat rejection shows significantly scattered data due to the multi-dimensional problem. While some parameters show general correlation trends of increasing or decreasing specific heat rejection with changes in input parameters, for other parameters these trends are much less pronounced.

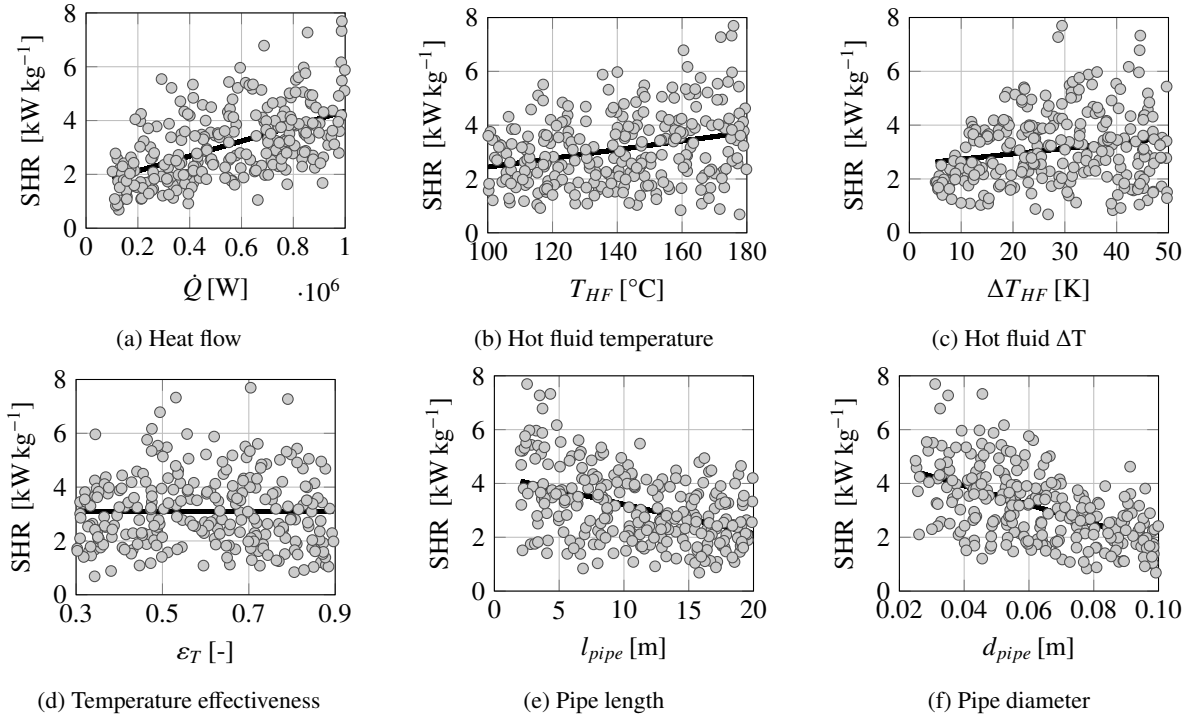

(a) Heat flow

(b) Hot fluid temperature

(c) Hot fluid ΔT

(d) Temperature effectiveness

(e) Pipe length

(f) Pipe diameter

Figure 10: Results of design space exploration with regard to scalability of the specific heat rejection

DOI: 10.13009/EUCASS2023-262

In conclusion of Figure 10, the illustrated results lead to the following recommendations from a TMS perspective to increase the specific heat rejection and thus reduce the TMS mass for a liquid cooled system:

- Managing higher heat loads by a single TMS yields benefits due to a relative decrease in pump and fan mass.
- Integrating the TMS within the components to reduce the routing of coolant fluids to achieve both lower pipe and lower hot fluid mass might be a potential key enabler. However, additional safety related considerations would have to be addressed.
- Increasing component operating temperatures and coolant fluid temperature difference lead to higher achievable specific heat rejection values.
- Considering the HEX design temperature of the air side as a design space variable is recommendable to achieve optimised systems.

At the same time, the TMS acts within the whole electrified propulsion system and will therefore be limited by the physical constraints of the individual propulsion system components.

4. Discussion

Starting from the design space exploration discussed in Section 3, results for dedicated application cases of electric propulsion systems are derived. As examples, the following use cases are discussed in more detail:

- Low Temperature Polymere Electrolyte Membrane (LTPEM) Fuel Cell (FC) system leading to a heat load of 600 kW at typical temperature levels of 80 °C to 90 °C for different fluids
- High Temperature Polymere Electrolyte Membrane (HTPEM) FC system leading to a heat load of 600 kW with varied temperature difference for heat pickup of 10 K to 30 K as well as varied pipe lengths to address integration aspects

For LTPEM FC systems, the generated heat needs to be managed at comparably low temperatures of 80 °C to 90 °C [26]. To prevent degradation, both LTPEM as well as HTPEM FC systems require, ideally, uniform temperature distributions across the fuel cells. For a limited temperature difference of 10 K, the results for two different fluids are given in Table 2 and Figure 11a.

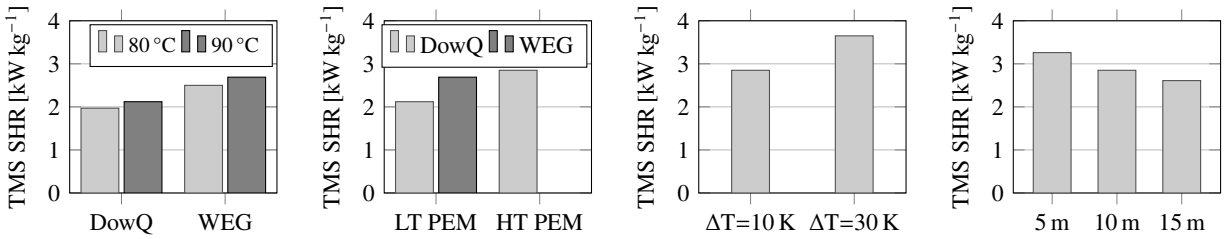

(a) Fluid type (b) LT PEM vs. HT PEM (c) Hot fluid ΔT (d) Pipe length

Figure 11: Specific heat rejection for different fuel cell application cases

An increase in operating temperature from 80 °C to 90 °C yields an increase of 7.5 % for the specific heat rejection for both fluids. At the same time, the investigation highlights the need for using fluids with high specific heat capacities as the required pumps are significantly smaller for lower volume flow rates which in turn yields higher specific heat rejection values.

For HTPEM FC systems, a higher operating temperature of 180 °C [26] compared to 90 °C of an LTPEM FC improves the sizing of components such as the heat exchanger and fan due to the larger air temperature differences as shown in Figure 11b and tabulated in Table 2. However, the operating temperature also restricts the available heat transfer fluids. While comparing the same fluids used for cooling (i.e. DOWTHERM Q), there is a significant increase in specific heat rejection from 2.12 kW kg^{-1} for an LTPEM FC to 2.85 kW kg^{-1} for an HTPEM FC application which corresponds to a 34 % increase. The improvement opportunity reduces to 6 % (2.69 kW kg^{-1} compared to 2.85 kW kg^{-1}) when using Water-Ethylene-Glycol based fluids used for LTPEM FC, which show better performance.

DOI: 10.13009/EUCASS2023-262

FC type	Fluid	T=80 °C	T=90 °C
LTPEM	DowQ	1.97	2.12
LTPEM	WEG-50 %	2.50	2.69
FC type	Fluid	T=160 °C	T=180 °C
HTPEM	DowQ	2.76	2.85

Table 2: LTPEM and HTPEM FC TMS specific heat rejection ($kW\,kg^{-1}$) across different fluids and operating temperatures

Both at absolute temperature level as well as for the relative improvements between the fuel cell types, significant improvements on individual component levels are required to achieve the target specific heat rejection rates of $5\,kW\,kg^{-1}$ to $20\,kW\,kg^{-1}$ at TMS level projected by Webber *et al.* [6].

Varying pipe lengths can be used to implicitly account for the integration of the TMS. Shorter pipe lengths of the total system herein indicate a higher degree of system integration and less distance between heat pick up and heat rejection. Similarly, long pipe lengths can be used to represent a centralised propulsion system with multiple distributed propulsors and a central heat management. For the investigated pipe lengths of 5 m to 15 m, a variation in specific heat rejection of up to 20 % can be observed for this variation in Table 3 and illustrated in Figure 11d. More integrated systems with shorter pipe lengths are therefore advantageous compared to systems requiring longer piping.

The hot fluid temperature difference can be used implicitly to describe serial cooling concepts as proposed by Link *et al.* [5] which identified a potential for higher specific heat rejection values with increasing hot fluid temperature difference. The results shown in Figure 11c as well as the tabulated data in Table 3 show a similar behaviour with increasing specific heat rejection values as a trade-off of fluid mass, heat exchanger and pump sizing.

Parameter	Value	SHR ($kW\,kg^{-1}$)
l_{pipe}	5 m	3.26
l_{pipe}	10 m	2.85
l_{pipe}	15 m	2.61
ΔT_{HF}	10 K	2.85
ΔT_{HF}	30 K	3.65

Table 3: HTPEM FC TMS specific heat rejection for different TMS assumptions

5. Conclusions

In this paper, a generic liquid based TMS was introduced to manage heat loads for electric propulsion systems for aviation. For this system, individual components such as the fluid, heat exchanger, pipes as well as fans and pumps have been modelled accordingly. The specific heat rejection as a ratio of rejected heat to system mass was reviewed as a key metric to characterise the system mass penalties besides a power ratio describing the required electric power to manage the heat flows.

While the fan and pump mass correlations are based on data sheets, the effect of these components onto the total system mass is significant and therefore also affects the achievable specific heat rejection. For both components this highlights the need for both weight optimisations and dedicated component development for large scale fuel cell applications in aviation. This is especially relevant for electric powertrain components running at low operating temperatures such as LTPEM FC.

The presented investigation showed that the TMS needs to be considered as a whole system during assessments. System design parameters such as heatflow, temperature levels and pipe dimensions, lead to trade-offs between individual components on both the air side as well as the liquid side.

General requirements to the TMS design can be derived with regard to: using the fluid with the highest heat capacity available for the given application, increasing component operating temperatures and temperature difference for heat pickup and thus increasing the air heat sink potential as much as possible as well as integrating the TMS and reducing the piping and fluid mass as much as possible. All of those factors lead to an increase of the specific heat rejection and thus a decreased system mass. However, the benefit of those improvements from a TMS perspective needs to be judged at overall system performance and mass level within the design process.

DOI: 10.13009/EUCASS2023-262

Especially for components operating at temperatures below 100 °C, it is also required to assess the trade-off between mass and power of the TMS since systems with a high specific heat rejection might lead to excessive power penalties.

6. Acknowledgements

The authors appreciate the valuable discussions with Sahil Bhapkar on heat exchanger sizing methodologies and with Caio Dias Fernandez on fan and pump mass approximations.

References

[1] Air Transport Action Group (ATAG). 2021. Waypoint 2050. https://atag.org/resources/waypoint-2050-2nd-edition-september-2021/

[2] Freeman, J., P. Osterkamp, M. Green, A. Gibson, and B. Schiltgen. 2014. Challenges and opportunities for electric aircraft thermal management. *Aircraft Engineering and Aerospace Technology: An International Journal*. 86/6:519–524

[3] Lents, C. 2021. Impact of Weight, Drag and Power Demand on Aircraft Energy Consumption. In: *AIAA Propulsion and Energy 2021 Forum.* AIAA 2021-3322.

[4] Gkoutzamanis, V., E. Spyros, O. Valsamis Mylonas, A. Kalfas, K. Kyprianidis, P. Tsirikoglou, and M. Sielemann. 2022. Thermal Management System Considerations for a Hybrid-Electric Commuter Aircraft. *Journal of Thermophysics and Heat Transfer*. 36/3 650–666.

[5] Link, A., J. Ludowicy, and M. Staggat. 2022. Assessment of a Serial Cooling Concept for HTPEM Fuel Cell Systems for Aviation Applications. In: *33rd Congress of the International Council of Aerospace Sciences*.

[6] Webber, H., J. Llambrich, and H. Davoudi. 2022. Thermal Management - Roadmap Report: FZO-PPN-COM-0019.

[7] Welstead, J. and J. Felder. 2016. Conceptual Design of a Single-Aisle Turboelectric Commercial Transport with Fuselage Boundary Layer Ingestion. In: *54th AIAA Aeospace Sciences Meeting*. AIAA2016-1027.

[8] Jansen, R., C. Bowman, and A. Jankovsky. 2016. Sizing Power Components of an Electrically Driven Tail Cone Thruster and a Range Extender. In: *16th AIAA Aviation Technology, Integration, and Operations Conference*. AIAA 2016-3766.

[9] Rheaume, J. and C. Lents. 2018. Design and Simulation of a Commercial Hybrid Electric Aircraft Thermal Management System. In: *2018 AIAA/IEEE Electric Aircraft Technologies Symposium*. AIAA 2018-4994.

[10] Rheaume, J., M. Macdonald, and C. Lents. 2019. Commercial Hybrid Electric Aircraft Thermal Management System Design, Simulation, and Operation Improvements. In: *AIAA Propulsion and Energy 2019 Forum*. AIAA 2019-4492.

[11] Palladino, V., A. Jordan, N. Bartoli, P. Schmollgruber, V. Pommier-Budinger, and E. Benard. 2021. Preliminary studies of a regional aircraft with hydrogen-based hybrid propulsion. In: *AIAA AVIATION 2021 FORUM*. AIAA 2021-2411.

[12] Chapman, J., S. Schnulo, and M. Nitzsche. 2020. Development of a Thermal Management System for Electrified Aircraft. In: *AIAA Scitech 2020 Forum*. AIAA 2020-0545.

[13] Chapman, J., H, Hasseeb, and S. Schnulo. 2020. Thermal Management System Design for Electrified Aircraft Propulsion Concepts. In: *AIAA Propulsion and Energy 2020 Forum*. AIAA 2020-3571.

[14] Bell, I., J. Wronski, S. Quoilin, and V. Lemort. 2014. Pure and Pseudo-pure Fluid Thermophysical Property Evaluation and the Open-Source Thermophysical Property Library CoolProp. In: *Ind. Eng. Chem. Res.* 53/6:2498–2508.

[15] Morrison, F. 2013. Introduction to Fluid Mechanics. Cambridge University Press. New York.

[16] Kays, W. and A. London. 1998. Compact Heat Exchangers. Krieger Publishing Company.

DOI: 10.13009/EUCASS2023-262

[17] Bachmann, P., P. Polte, and V. Gümmer. 2022. A preliminary design method for corrugated louver fin and rectangular offset strip fin heat exchangers. In: *Deutscher Luft- und Raumfahrtkongress*.

[18] Shah, R. and D. Sekulić. 2003. Fundamentals of heat exchanger design. John Wiley & Sons.

[19] Manglik, R. and A. Bergles. 1995. Heat transfer and pressure drop correlations for the rectangular offset strip fin compact heat exchanger. In: *Experimental Thermal and Fluid Science*. 10.2:171-180.

[20] Parker Hannifin Corporation. 2009. Aircraft Engine-Driven Pumps (Data Sheet). https://www.parker.com/content/dam/Parker-com/Literature/Hydraulic-Systems-Division/HSD-literature-files/HSD-1-.product.spec.sheet_EngineDrivenPumps.pdf.

[21] Eaton. 2008. Main Gear Fuel Pump (Data Sheets Collection). https://www.eaton.com/content/dam/eaton/products/pumps/aerospace-fuel-pumps/documents/eaton-main-gear-fuel-pump-brochure-tf600-52_en-us.pdf.

[22] tecomotive. 2023. Pierburg Water Pumps. https://www.tecomotive.com/de/produkte/pumpen.html.

[23] Meggitt Defense Systems. 2021. Military & Aerospace Fans Catalog. https://meggittdefense.com/wp-content/uploads/2021/12/Fans_Catalog_By-Item-Number_2021-1.pdf

[24] Orientalmotor. 2023. Axial Fans. https://www.orientalmotor.com/cooling-fans/axial-fans.html

[25] Teichel, S., M. Dörbaum, O. Misir, A. Merkert, A. Mertens, J. Seume, and B. Ponick . 2015. Design considerations for the components of electrically powered active high-lift systems in civil aircraft. In: *CEAS Aeronautical Journal*. 6.1:49–67.

[26] Kazula, S., S. de Graaf, and L. Enghardt. 2023. Review of fuel cell technologies and evaluation of their potential and challenges for electrified propulsion systems in commercial aviation. In: *Journal of the Global Power and Propulsion Society*. 7:43–57.